Untethered and Modular Inflatable Robots for Lunar Operations

Final Report for 2024 NASA BIG Ideas Competition by BYU Engineering Team

James Wade[1], Chris Paul[1], Mihai Stanciu[2], Jared Berger[1], Spencer Stowell[2], Henry Smith[1], Kaitlyn Bell[1], Isaac Weaver[2], Simon Charles[1], Logan Yang[1], Ashleigh Cerven[1], Jayden Coe[1], Brian Bodily[1], Lais Oliveira[1], Eli Francom[1], Annie O'Bryan[1], Bryce Parkinson[1], Ivyann Running[2], Jake Sutton[2] Adam Rose[2], Katie Varela[2], Nathan Usevitch[3], Marc Killpack[3]

Space Grant Affiliation: Utah NASA Space Grant Consortium
Space Grant Director Information: Dr. Joseph Orr
joseph.orr@hsc.utah.edu, 801-573-2091

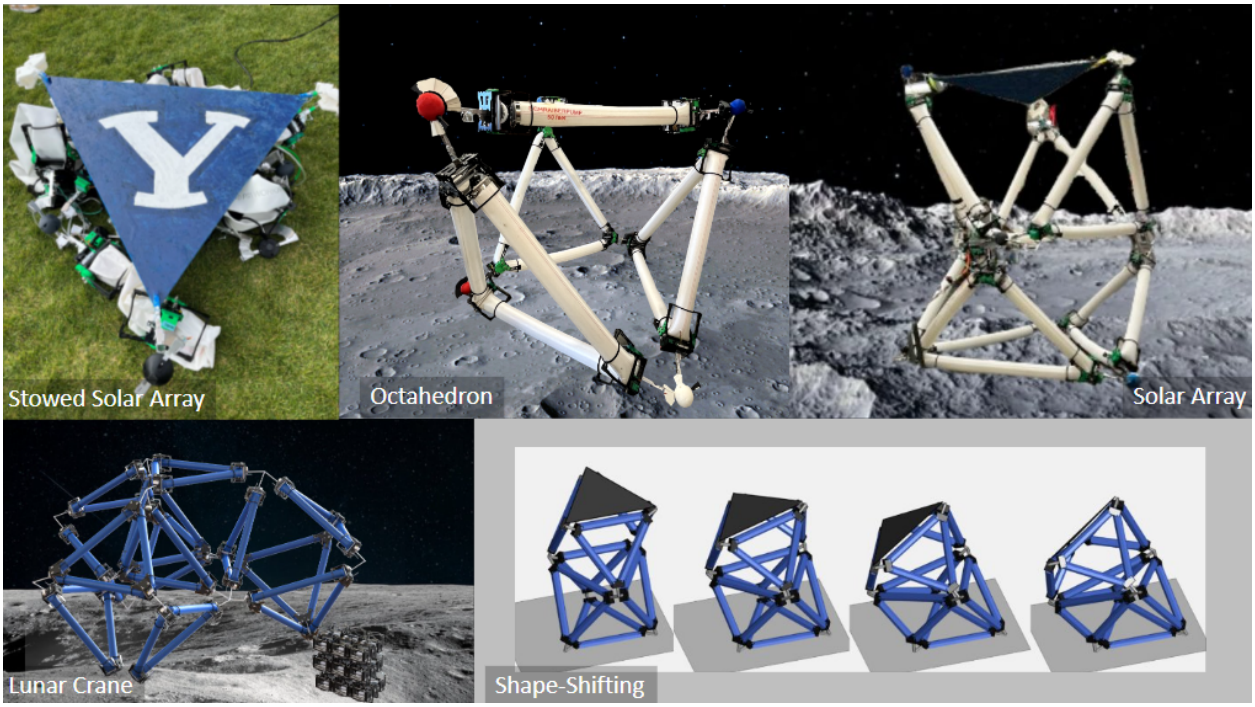

Brigham Young University
Ira A. Fulton College of Engineering

1 Department of Mechanical Engineering, Undergraduate Student
2 Department of Mechanical Engineering, Graduate Student
3 Department of Mechanical Engineering, Faculty Advisor

Faculty advisor signature of approval: x _____

Contents

Brigham Young University: Untethered and Modular Inflatable Robotics for Lunar Operations

Concept Synopsis

- Inflatable robot with the ability to adjust the relative bent shape of inflated tube configurations by the motion of motor driven rollers untethered to an air supply
- Modular triangular components with the ability to be reconfigured into a variety of systems according to use case

Image Depicting Concept

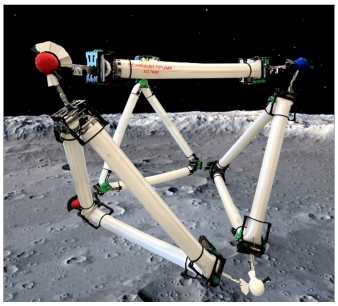

Innovations

- Compact and lightweight node design using topology optimization and a self-lubricating polymer
- Swappable mechatronic components with external status visualization for each roller and dynamic modeling capabilities
- Novel spherical joint design
- Airtight plug system that can accommodate high tube pressures

Verification Testing Results and Conclusions

- Verified that the system can operate with tube materials similar to those that can withstand lunar elements through thermal testing, sandblasting, and UV testing
- Validated developed dynamic model through collecting and analyzing positional data
- Compression and shearing testing to determine strength requirements for joint stability
- Verified a linear relationship between higher current draw and higher tube PSI and as a result, optimized the tube PSI range to minimize the average current draw

1 Executive Summary

1.1 Operational Scenario

Sustained life on the moon requires robotic structures that can perform a variety of different tasks. Habitats will need to be built. Solar panel arrays will need to be positioned. Machines will break and need repair or modification. Having astronauts perform all these tasks is dangerous and time-consuming, so having general-purpose robots is a commonly proposed solution. Conventionally, rigid-body robots and materials are the candidates for lunar applications. But these candidates' greatest strength is their greatest weakness—they are rigid, heavy, hard to stow, and unadaptable for a design other than the one intended. So what is to be done?

1.2 Overview of Proposed Technology

At BYU we have developed a versatile robotic system that is lightweight, can be stored in a small volume, and can be reassembled for a variety of tasks. Our robot's design features an inflatable, modular robotic system that combines aspects of soft and traditional robotics. Our design consists of inflatable beams that are bent into triangles, with motor-driven nodes at the corners, pinching the tubing. These triangles can be combined into octahedra and even larger structures. Each node has four steel rods that, when rotated by the motor, move tubing from one side of the node to the other. This motion, combined with similar coordinated motion in the other nodes, can morph the shape of the robot into many load-bearing and task-performing applications. Our research group is building the isoperimetric robot developed by our faculty mentor, Dr. Nathan Usevitch [1]. To build upon this existing technology, we will demonstrate using two octahedra to direct a solar or antenna array.

1.3 Testing and Verification

This robot can be broken down into subsystems, namely the tubes, the rollers, the joints, and the dynamics. Testing for each of the subsystems individually helps affirm that the robot overall will be able to fulfill its purpose and be prepared for the lunar environment. Some of the testing focused on the environmental aspects, such as UV exposure, thermal effects, and lunar regolith, while other tests were performed on the mechatronics and load-bearing properties of the robot in its tubes, rollers, and joints. The Autoliv facilities in Ogden were extremely helpful with their thermal chambers for tube testing. Our robotics lab is also equipped with a motion-sensing array to track the movement of our robot in 3D space, allowing us to begin verifying the dynamic model we constructed for our robotic system. Our final verification consisted of building an operational robotic solar panel mount that consisted of 6 motorized triangles.

1.4 Impact of This Technology on Lunar Exploration

Through the continual development and implementation of our design, this robot could change the future of lunar habitability. Our robot can shape-shift through kinematic controls, be structurally reassembled into even more configurations, transport heavy loads, and autonomously direct a solar panel array. It is lightweight (with a deployed-to-stowed ratio of 5:1), has minimal operation risk for astronauts, and can even locomote like an 8-sided die. Our robot provides adaptable alternatives to rigid structures. It is not hyperbole to say that the updated isoperimetric robot will be one of the most versatile robots ever created. In short, our design has the potential to alter the future of the lunar missions as they are currently imagined.

2 Problem Statement and Background

It has been almost 50 years since astronauts last walked on the lunar surface. The United States of America needs to achieve the earliest possible lunar landing to maintain and expand the scientific advancements and leadership established in the period since the Apollo Missions. The sooner humanity achieves sustainable life on the Moon, the sooner astronauts can reach Mars. The Artemis missions are designed to sustain long-term astronaut life and exploration on the lunar surface. They aim to establish a lunar base camp on the lunar South Pole, from which astronauts can explore nearby regions and, eventually, the entire Moon. However, such endeavors require large robotic structures capable of completing a variety of tasks, including tasks that may not be known beforehand. Robotic structures with these capabilities do not currently exist.

Conventional robots and reconfigurable structures designed for the Moon require a large volume and weight capacity in the spacecraft, both limited commodities. Once transported, these artifacts are designed to fulfill one specific purpose. Permanent human presence requires lightweight, adaptable, robotic structures.

Soft, pneumatically-driven robotics offer significant advantages as candidates for lunar structures and robots. Inflatable soft robots can be packed into a small volume and are lightweight compared to conventional materials. The compliance and adaptability of soft robots make them suitable for operating in unstructured environments and alongside people. On the Moon, where safety, volume, and versatility are highly important, soft robotics may find an innovative niche. NASA's BIG Idea Challenge for 2024 incentivizes the creation of new, innovative soft robot designs. However, inflatable robots also have intrinsic challenges: inflating and deflating actuators are energy inefficient (commercial compressors operating at peak efficiencies of <40% [2]), and on the lunar surface ambient air is not available. Inflatable robots must also be adapted to the harsh environment of the lunar poles. If soft robotics can overcome these challenges, they could provide a clear advantage over the conventional rigid-body robots found today.

We have developed a robotic system that captures the capabilities of soft robots, while operating with a fixed volume of air and being capable of forming a variety of complex shapes. Our soft robot provides an adaptable structure that can be reconfigured to perform many robotic tasks, eliminating both the large volume and weight requirements in delivery to the lunar surface. The robot's primary structure is inflatable fabric beams, and the ratio of deployed-to-stowed volume for the entire robotic structure is 5:1. Our robot enables large-scale structures, with our proposed solar panel mount standing 2.4m tall, and our crane standing 2.2 m tall. Our truss-like structure is adaptable in two ways:

1. **Shape-Changing Ability** - The robot's ability to, through the coordinated motion of its motors, change the relative lengths of each tube and create various load-bearing shapes. The many degrees of freedom, coordinated by a kinematic controller, enables the robot to perform a variety of tasks and adapt to changing conditions and terrain without intervention.

2. **Modular Reassembly** - The ability for an astronaut to detach and replace an inflated triangular module into any combination of shapes. The device consists of modular triangles that can be reconfigured by the astronaut into several different base robot shapes, making it capable of completing and adapting to different tasks and terrain that may not be known prior to the mission. The modular construction also allows a single element of the robot to be replaced if it is damaged, enabling robustness through modularity.

The robot is composed of multiple inflated fabric tubes folded into triangular shapes in a truss-like structure. Each triangle consists of a long inflatable tube and three motorized modules at the nodes of the triangle. The motorized nodes (consisting of a DC motor and rollers) roll along the length of the tube, lengthening one edge of the triangle and shortening the other. By attaching multiple triangles in geometric shapes, flexible structures are created that can adapt their shape to the desired need. Our faculty advisor's previous research showed that an octahedron-shaped truss made from these triangles was capable of locomoting like an 8-sided die [1]. Once deployed, this system has a constant inflated volume, and no external air compressor is necessary, allowing for untethered movement. The bulk of the mechanical work is performed by electric motors, providing a higher energy efficiency than a system of repeated inflation. Furthermore, this design is compactly stored when deflated, optimal for transport into space (see Figure 1).

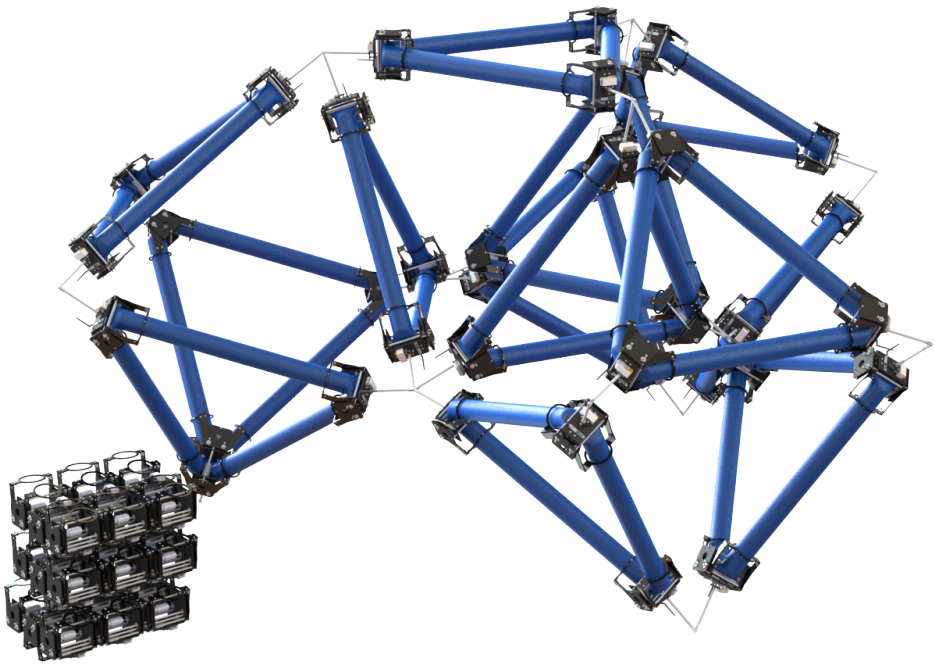

Figure 1: A to-scale render of the deployed-to-stowed volume ratio of our lunar crane design

To build on this existing technology and optimize it for use on the Moon, our research group has demonstrated the following results:

- Developed a physical prototype of a large inflated truss robot. The robot stands 2.7m tall, and can stow in a volume 1/6 its deployed volume.
- Developed a simulation tool that allows us to explore different configurations of the robot for different tasks.
- Developed a novel spherical joint that allows multiple triangles to be connected together while sharing a center of rotation.
- Develop a quick-release joint system that allows an astronaut to quickly reassemble the triangles into different structures based on the required task.
- Measured the dynamic performance of the robot. This will allow future controllers account for the natural compliance when the robot is being controlled on the moon.
- We have tested the device for performance under large swings of temperature as might be experienced on the moon.

Our goal is to expand the possibilities of soft robotics for advanced lunar missions and the long-term establishment of life on the Moon. Currently, the only options for lunar devices are heavy, expensive, and inflexible in performing a task other than the one they are designed for. In a harsh environment like the Moon, adaptability is key. To overcome this challenge, we are proposing to synthesize the advantages of traditional robotics (robustness, untethered motion) with the unique strengths of soft robotics (low inertia, small packing volume). Only through this combination of characteristics can humanity unlock the full potential for sustained life on the Moon.

3 Project Description

3.1 Overall Description

The "New Frontier" of space is being approached differently than it has been in the past. There is interest in being able to develop on the Moon, but the required launch volume to transport machinery and other building materials to the lunar surface requires extreme expense.

The solution to these problems can be found with adaptable, soft robots. Soft robots can be inflatable, autonomously shape-changing structures that are lightweight and can deflate and stow in small volumes. Nevertheless, soft robots have challenges of their own—they require a source of air that is not available from the lunar environment, and they are relatively energy inefficient (commercial microcompressors of air often operate at peak efficiency of only <40% [2]). In addition, load-bearing inflatable members are typically limited to balloon-type shapes that are difficult to constrain into useful configurations.

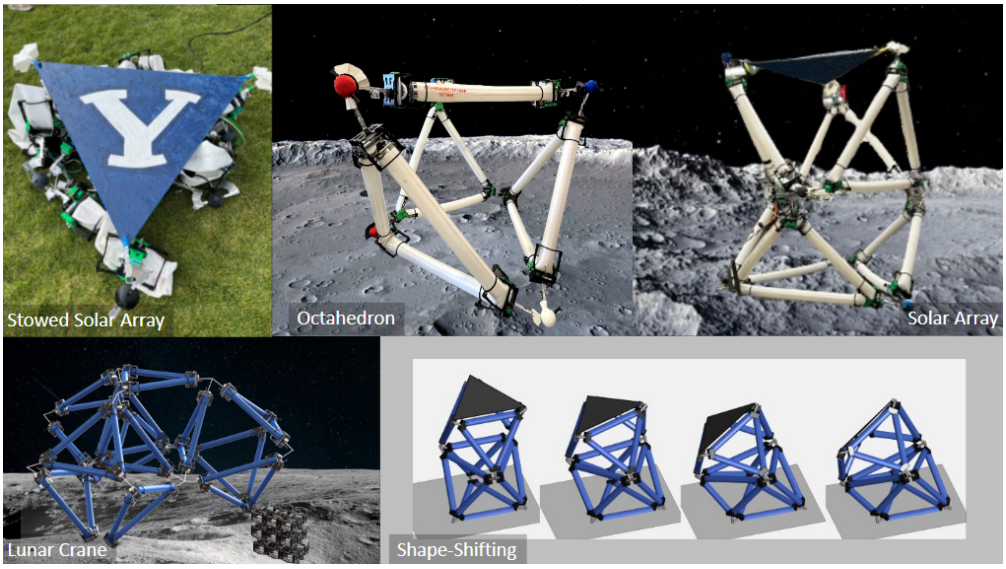

Figure 2: A lunar crane stowed (top left), a deployed octahedron (top middle) and a solar panel mount (top right). and an octahedron (bottom right) composed of the proposed robotic triangles. For the lunar crane, the deployed volume of the solar panel mount is 6x size of the deflated nodes. Using its motors and our control algorithm, the robot can change its own shape (bottom right)

We propose a robotic system that can create lightweight, adaptable, and powerful robotic structures on the Moon, shown in Figure 2. This modular system comprises truss-like robotic triangles, each formed by a continuous fabric tube routed through three robotic roller modules. Deflated, these triangles can be packed down to the volume of only the roller modules. Upon inflation, the roller modules pinch the tubes, creating corners by reducing the bending stiffness of the tube. The triangle changes shape as electric motors move the modules along the inflated tube, moving the pinch point while lengthening one edge and shortening another. This manipulation does not change the overall inflated volume, meaning that after the initial inflation, no source of compressed air is needed. Because the primary source of work for the robot is electric motors, the robot can have a far higher energy efficiency than a soft robotic system relying on compressing air (electric motors can achieve efficiencies of >90% [3]). Multiple triangles can connect through spherical joints on the roller modules, enabling the creation of large 3D structures for a variety of shapes and functions. This design enables the following key advantages:

- High ratio of stored to deployed size- our robot has a ratio of deployed to stowed volume of 6.2
- Untethered operation- Our robot remained inflated in the lab for over a week without substantial leaking
- Task flexibility through shape change and modular reassembly
- Energy efficiency

- Robustness through modular reassembly (broken components can be replaced with other modular components)

The system proposed here allows for a wide variety of robots to be created, though this work focused on using two octahedra to create a solar array.

This robotic system can adapt itself to changing environments or tasks in two ways: shape change via onboard motors, or modular reassembly with the assistance of an astronaut. The robot will not autonomously change its connections (i.e. the joints) between triangles to form a new assembly. However, this proposal will lay the groundwork for future systems that could combine both their shape-change ability and their ability to be reassembled to form robots that autonomously change the internal connections between the robotic triangles.

4 Design Analysis and Justification

Our robot is composed of four distinct subsystems that work together to create this interesting functionality, a graphic pointing out three of these four subsystems is shown in Figure 3. As shown, inflatable tubes provide the structure of the robot, allowing it to hold its shape while remaining compliant. Mechanical rollers provide bending points along the tube, enabling the robot as a whole to change its shape. One tube and three rollers (two active and one passive, described in the architecture section below) create a single, shape-changing triangle of our robot. Spherical connection joints are needed to connect multiple triangles while allowing the triangles to shift relative to each other as the overall robot moves. This movement is modeled, visualized, and planned by the kinematics and dynamics subsystem. During this project, our team sought to deliver marked improvement on each of these subsystems by adapting them for the Moon. Each of the sections below describes our team's improvements to each of the subsystems.

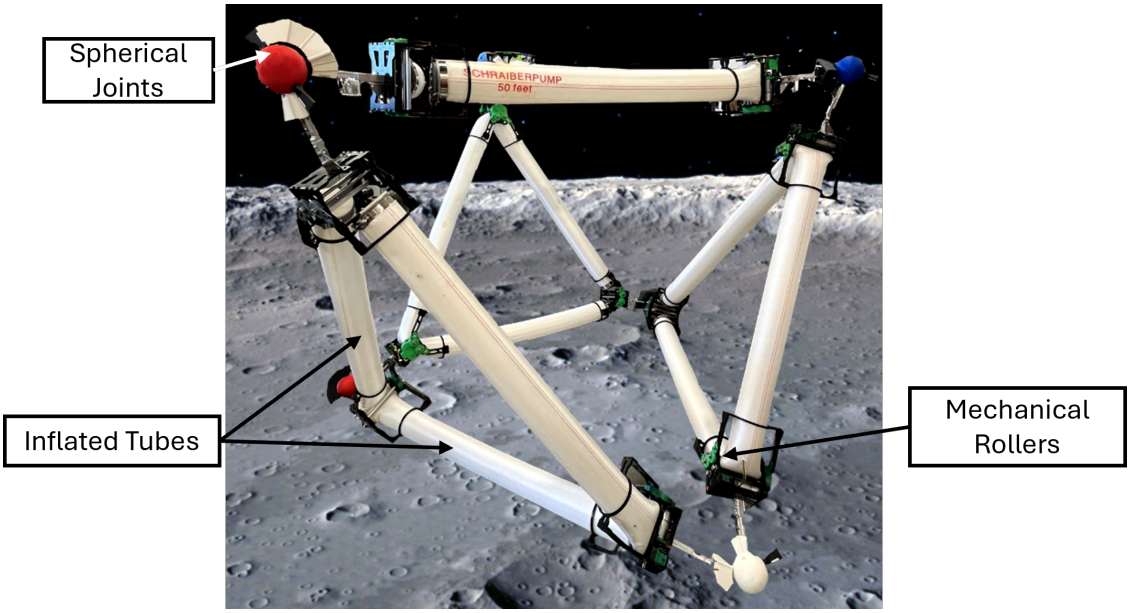

Figure 3: A closer view of a single assembled octahedron of our robot. The design consists of four subsystems (dynamics subsystem not labeled on the Figure) working together to create motion and complete tasks.

4.1 Roller Design

4.1.1 Function

The roller units constitute the subsystem that bends and actuates the tube in the desired shape. There are two configurations, active and passive, for the roller unit subsystem, each with different functions.

Both roller unit configurations must be light enough to not over-encumber the structure and strong enough to withstand stresses from the spherical joint interface. The active unit must sustain the tension

forces created by the pressurized tube. Additionally, the passive roller unit must resist stresses from the spring-back effect caused by bending the pressurized tubes from their natural linear state into triangles. These stresses are balanced in the powered rollers because the tube continues on both sides.

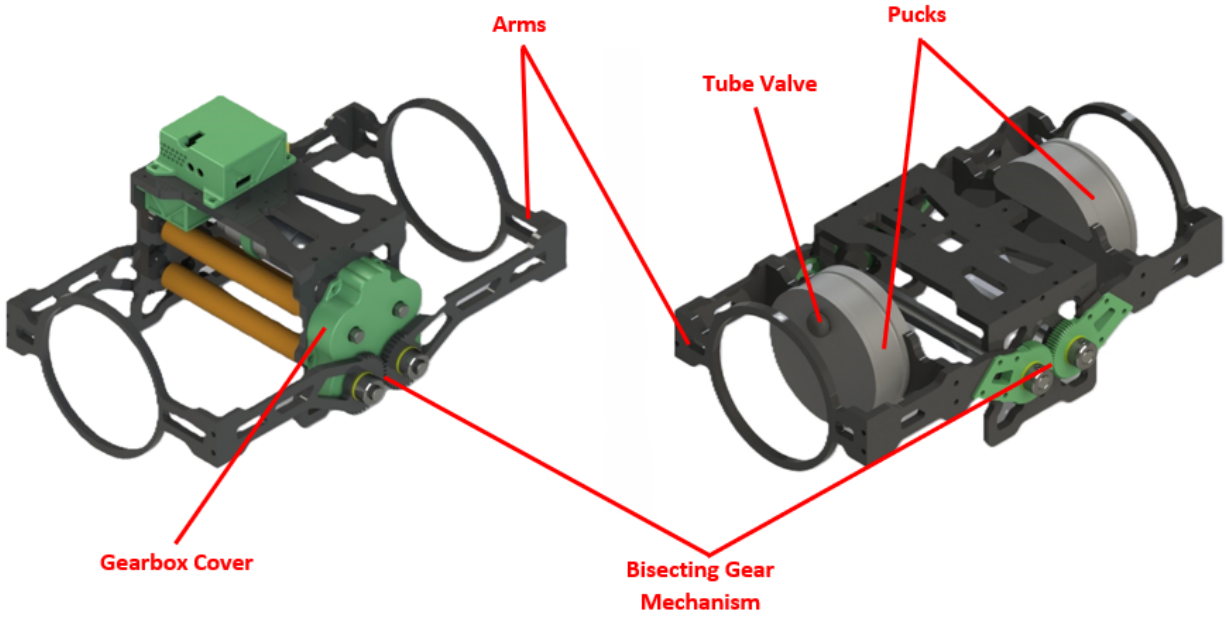

Figure 4: Renders of the active (left) and passive (right) roller units with some important nomenclature highlighted. The inside of the gearbox is showcased in Figure 5

The function of an active roller unit is to move along a tube the distance specified by the controller without any slippage or jamming so that the structure can change its shape according to the kinematic protocol. Moreover, the active roller unit must be energy efficient to increase the battery life of the robot while still being strong enough to avoid yielding under the pressure loads exerted by the tube.

The passive roller unit is a simplified version of the active unit and its function is to connect the two ends of the tube, by sealing the tube around the pucks, so that each triangle is one continuous substructure. For this, the passive unit must have additional features that allow for interface with the pucks at both ends of the tube.

After developing the kinematics model for the robot, it was determined that each triangle needs only two active and one passive roller to achieve a full range of motion for a given triangle.

4.1.2 Architecture

Active Roller

The active roller's architecture can be broken down into 4 sub-assemblies: chassis, roller, and long and short arms.

The chassis comprises three parts, two sides and the top which are laser-cut out of Delrin and have some features machined for precision. Besides attaching modules such as the PCB, battery, motor, and spherical joint interface, the function of the chassis is mainly structural. The two sides on each chassis were machined together so that the roller shaft holes are perfectly concentric. This is important because the gears that drive the shafts must mesh precisely and the shafts need to remain concentric with the holes in both sides to minimize friction with the Delrin. Together with the top plate, an aluminum spacer at the bottom of the chassis ensures that the two sides are parallel and adds structural integrity.

The 4 rollers are precisely machined carbon steel shafts onto which a natural rubber sleeve is attached to increase traction with the tube as it travels through the unit. The shafts need to be strong enough to not deflect under the loads exerted by the pressurized tube. These loads were calculated using a tube pressure of 15 psi and the projected area of the rollers onto the tube. Using a custom-made adapter, the acetal gears

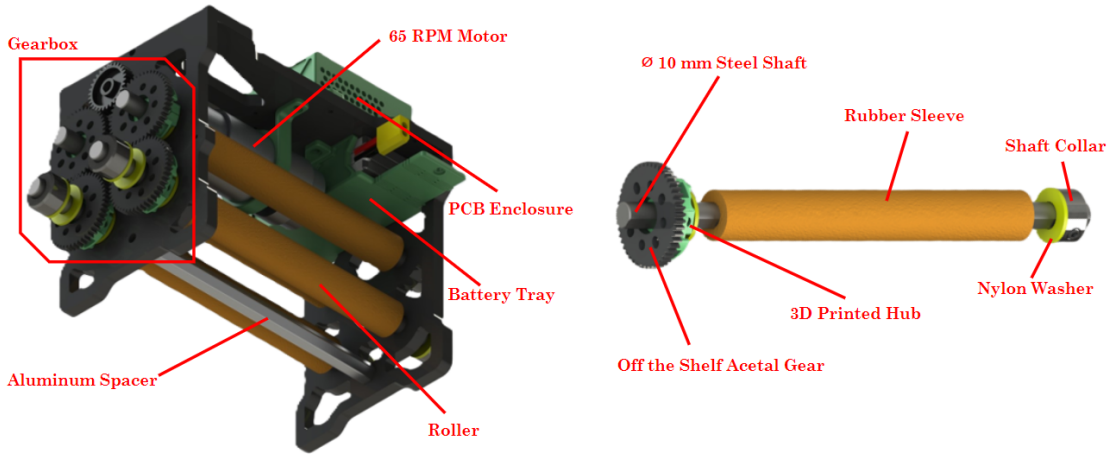

Figure 5: Mechanical architecture for the active roller unit (left) and roller subassembly (right)

are attached to the shafts which actuate each other to create the pulling motion that runs the tube through the unit.

The purpose of the arms is to ensure that the angle at each vertex of the triangle is bisected so that the top plate of the roller unit remains parallel with the part of the tube that is being rolled through the unit. This is done by implementing a geared mechanism that enables the arms to actuate each other as the tube bends. The length difference between the two arm configurations (short and long) is so that they may fold into each other during stowing.

Passive Roller

The passive roller unit is composed of the same sub-assemblies as the active unit, only that they are simplified since the passive unit does not require a motor, gearbox, or electronics. Moreover, since the tube does not run through the passive unit, only two shafts without the rubber sleeve are being used. These shafts were kept in the design because the passive unit still requires the two arm sets.

Redesign

To achieve the design objectives, the roller unit has been redesigned to be lighter, have increased traction with the tubes, and experience minimal friction within its gearbox and with the chassis while remaining strong enough to support the design loads derived from the tube pressures.

To minimize mass on the two configurations of the roller unit, topology optimization techniques were run on most of the Delrin parts (see Figure 6). The steel spacers that were used in the older version of the roller unit were changed to Aluminum ones since they will provide the same structural integrity. Moreover, to improve the simplicity of the design and to reduce its weight, bearings were removed and the shafts rotate within the Delrin itself since it is a self-lubricating polymer. This has resulted in significant weight reductions as seen in Figure 7.

To increase traction between the tubes and the roller units, each roller was equipped with natural rubber sleeves that are constrained so as to not slide on the steel shafts. This has fixed the issue of tubes slipping against the steel shafts as the tube is run through the unit.

To minimize friction in the gearbox, the side plates of each chassis were machined precisely together so that the distance between the shaft holes match the pitch diameters of the gears so that they mesh properly. This ensures that there is no undesired interference between the teeth of the gears increasing the friction in the mechanism. By minimizing the friction between gears, the torque, and thus the current, required by the motor to overcome this friction is also minimized, making the system more energy efficient and increasing its battery lifetime.

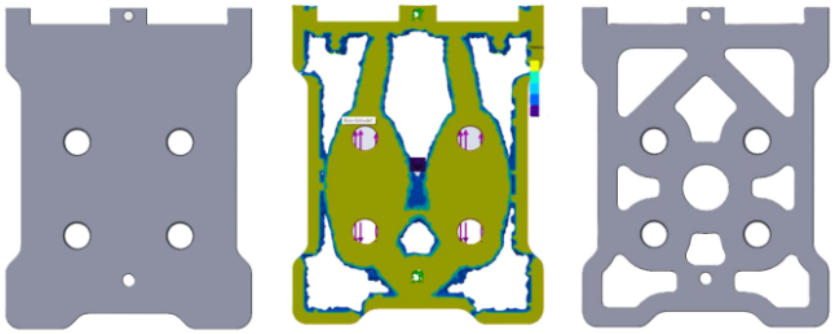

Figure 6: Topology optimization performed on the side plate for the active roller unit. The plate on the far-left side weighs around 110 grams and the one on the far-right side weighs around 76 grams.

Percent Weight Reduction at Unit Level		
Old Unit Design	New Active Unit Design	% Weight Reduction
3.14 kg	1.98 kg	37%

Percent Weight Reduction for Triangle Configuration		
3x Old Design Units	2x Active + 1x Passive Units	% Weight Reduction
9.42 kg	5.36 kg	43%

Figure 7: Table showcasing the weight savings per roller and triangle

4.2 Tube Design

The primary structural component of the robot is comprised of inflatable tubes. These straight tubes are approximately 12 feet in length and 4 inches in diameter, that go through rollers, causing them to bend into their triangular shape. There is one layer of material that is rigid enough to provide structural support for the robot, but flexible enough to run through the rollers. Each of the tube ends is secured with a plug and connected to a passive roller and can be deployed with no additional assistance once the inlet is properly set up.

Due to application and manufacturing constraints, the final tube design utilizes single-jacket polyurethane firehose tubing. Compared to many other elastomers, polyurethane has high tensile strength, low weight, excellent tear and abrasion resistance, and experiences little degradation from sunlight or ultraviolet exposure [4]. Low weight, high resilience to ultraviolet light, and abrasion resistance are essential to success in the lunar environment. High tensile strength and tear resistance extend the operating lifetime of the tube as the roller modules pressurize, pull, and compress the tubes during active operation.

Additionally, other considered materials such as ethylene propylene diene monomer (EPDM), Denier nylon, acrylonitrile butadiene copolymer (nitrile rubber), or chlorosulphinated polyethylene (Hypalon) were only available for purchase in sheets instead of tube form. Filament-wound polyurethane firehose satisfied many of our material and manufacturing constraints. The specific tubing we used for most of our prototyping and testing could withstand temperatures from 85 to -35 degrees Celcius, working pressures of 145 psi, and bursting pressures of 435 psi. These pressure ranges granted us a generous safety factor of ten during regular operation.

However, limitations included a narrow thermal range of operation and extensive sand retention during sandblasting due to the external polyester weave. To address this, we elected to use the Denier Nylon material as an outer tube to protect from the lunar environment. The Denier Nylon was not airtight enough

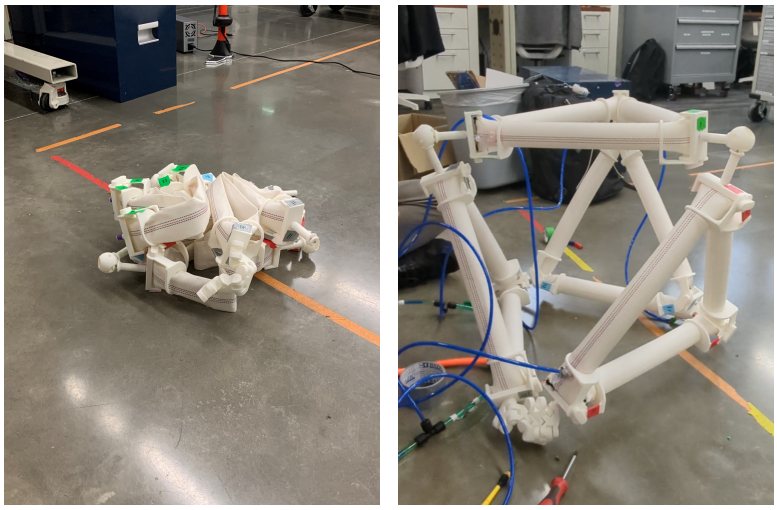

(a) *(b)*

Figure 8: Stowed Model Octahedron vs Inflated Model Octahedron

to use by itself, so the combination of the inner (firehose) tubing and the outer (Nylon) tubing is recommended to ensure that it can endure the temperature ranges, hold the air pressure, and withstand the lunar environment.

Plug

The woven tubes are capped on each end with a Stereolithography (SLA) printed plug made of Formlabs PLA Tough resin (called Pucks in Figure 4. Each plug has an indentation along the circumference with enough room for a strip of 3M VHB Butyl tape to fit inside which functions as an airtight sealant when a hose clamp is connected. The tape is soft enough to deform and fill all crevices, both in the SLA print and on the fire hose tubing, and also contains a mild adhesive that increases the friction between all surfaces at that interface. When properly tightened, the hose clamp crushes the butyl tape enough for the clamp ring to rest on the lower notch of the plug, further reducing the likelihood of slippage. When the tube is pressured, the plug is pushed away from the body of the tube, placing the tape in shear where its adhesive force is strongest.

The plug has a hollow design to reduce the weight, with a convex surface on the bottom to improve its resistance to deformation under load from the pressure inside the tube. This feature was added after observing significant deformation in a flat-bottomed plug during sustained loading over a week interval. Support pillars are included on the interior of the plug to provide additional support and prevent similar failures in the future. PLA tough was chosen as the plug material because of its increased ultimate strength compared to standard PLA. No measurable leaking has been observed through the SLA plugs. Each plug weighs 137 grams.

One plug of each pair has a through-hole to allow for a tire valve stem. This provides the orifice through which we fill each tube from a pressurized air supply. The valve stem is a commercially available part typically used in automotive tires, and it creates an airtight press-fit seal without the use of adhesives. Once the valve is in service, the pressure of the tube behind it increases the holding force inside the plug and further improves the seal's quality.

Deployment

To stow the robot compactly, we designed our tubes to be flexible and maneuverable enough to nest closely with the rollers, optimizing the robot's stowed to inflated ratio. To ensure we have the best triangular arrangements and stowing configuration, we tested both triangle and octahedron arrangements. We created a scale model of the octahedron structure to test deployment, shown in both a deflated and inflated state in Figure 8. We tested the relationship between triangle pressure and joint/roller mass at different triangular shapes to determine the best shape that each triangle should have in the octahedron and solar array. To

determine the best way to stow the robot so that it does not require human interference or guidance when inflating we experimented with various stowing configurations on a scaled down model robot. Each tested configuration consisted of a different way of folding the triangular components. Some of these configurations included wrapping the tube around a node, fan folding the tube, and scrunching the tube and nodes together. After inflating each arrangement, we determined that making one fold on one side of a triangle for each component in the octahedron, as shown in Figure 8a, was easiest to inflate without human interference while still maintaining a limited stowed volume. We found that the robot had a stowed to deployed ratio of 1:6.23 when we tested this arrangement on the full scale solar array.

4.3 Joint Design

A difficulty in the design of truss robots is the interface between truss members that allow for three rotational degrees of freedom (pitch, yaw, and roll). For a simple octahedron, clevis-pin joints at the geometric vertices can be used to allow four triangles to operate as a robotic octahedron [1]. When a third connection is needed, as is the case for the stacked octahedron "solar array" configuration, a pin joint is no longer viable. We needed a new joint design to connect three or more triangles. Past work in variable topology trusses has led to the innovation of different multi-link spherical joints. However, many of these designs do not provide adequate ranges of motion for our intended robot design or are not reconfigurable [5]. Others are highly reconfigurable, but contain many rubbing surfaces and crevices that could be problematic with lunar dust [6, 7].

To overcome mobility challenges, our initial joint design focused on two functions: maintaining a virtual center for multiple connections and reducing friction in the joint by utilizing compliant mechanisms.

We worked with BYU's Compliant Mechanisms Research group to design a novel compliant spherical joint that would be both reconfigurable and resistant to lunar dust. Compliant mechanisms are an attractive option because they eliminate the need for lubrication, reduce friction, and are more resistant to wear from lunar dust than designs that have surfaces rubbing against each other. The resulting joint enables multiple "arms" (see Figure 9) to be attached to a central node, with each arm having three rotational degrees of freedom and a high range of motion. Each arm consists of an array of panels, with adjacent panels joined by a compliant hinge. All the hinge axes intersect at the virtual center of the joint.

We tested a variety of materials as potential compliant hinges, including Kevlar, polyimide tape, carbon fiber, polypropylene, and aluminum sheet metal. For the panels, we experimented with materials such as PLA, carbon fiber PLA, and carbon fiber (see Figure 9). Due to the significant amount of parasitic deflection experienced in both compressive and tensile tests, we made the central connecting node a sphere to function as a compressive contact point and pre-strained the arms to resist deflection under tensile loads.

In parallel to compliant joint development, we tested the kinematics of the spherical joints with aluminum linkages. These linkages followed the same geometry of the compliant arm designs, with panels machined from aluminum and connected with steel pins (shown in Figure 9e). Ultimately, we decided to use the aluminum joint design because it is sufficiently strong and provides an appropriate range of motion for the robot. The pin hinges introduce friction to the joint, so a covering can be made to protect against the abrasive nature of the lunar regolith. Please refer to the Path to Flight section for a description of future work related to the joint covering and compliant joint design.

Connectors

We made the connection between the joint arms and the rollers out of aluminum and steel. We designed it to be sturdy and easy to attach and detach while under load. Previous designs used various methods to account for lunar dust (such as allowing space for dust buildup and avoiding sliding parts against each other), but as we prepared to build our prototype we shifted focus to something that was strong and simple to make and use. While using the joint regularly during reassembly and testing, we determined that it can be attached and detached in around 15 seconds.

4.4 Mechatronic System Design

The mechatronic system of the robot was designed for several key success measures. The mechatronic components on each roller need to provide power to the motors, track and control the position of the rollers along the tube, and communicate via radio with other rollers. The system needs to use interchangeable components that can be quickly changed to enable quick iterations and needs to be as light as possible to

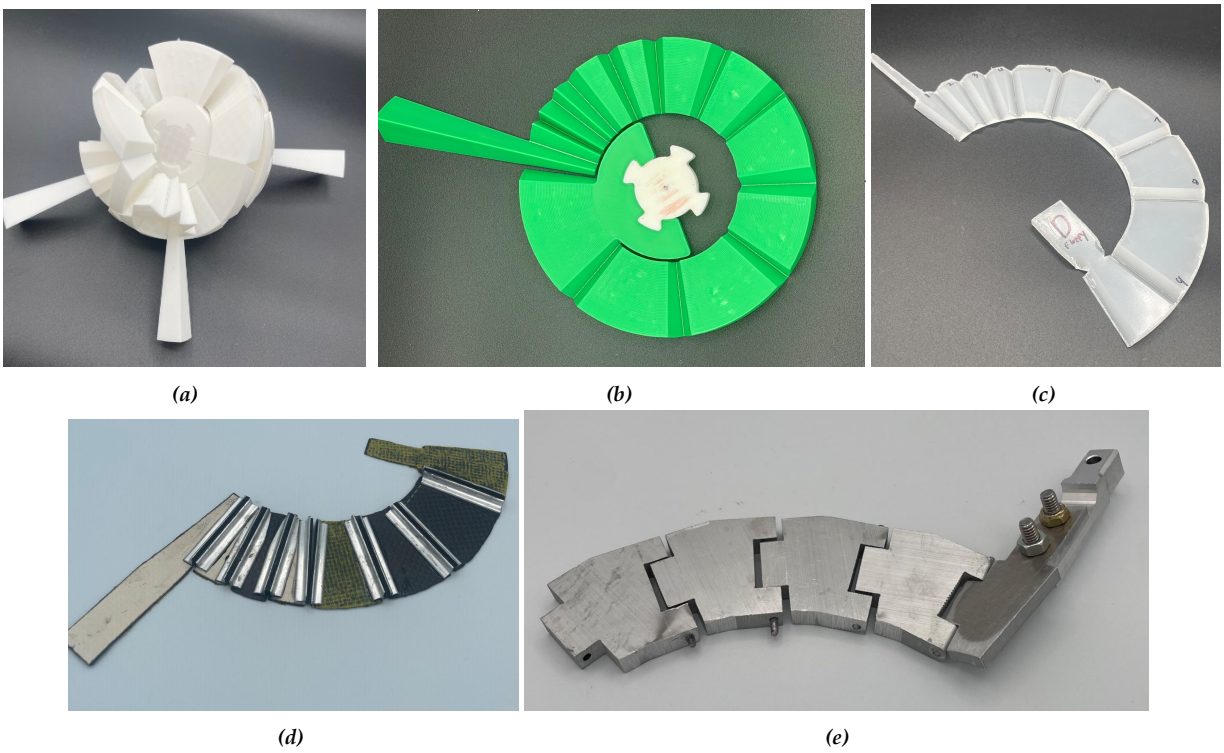

Figure 9: (a) A model of multiple arms connected to a central node. These arms connect to the inflatable triangles. (b-e) Iterations of materials and geometries for the arms. (b) PLA with living hinges. Segments add to 360°. (c) Polypropylene with living hinges. Segments add to 180°, which was shown to reduce crowding without significantly inhibiting ROM. (d) Carbon Fiber with carbon fiber Lamina Emergent Torsion (LET) joints. (e) Aluminum with steel pin joints.

mimic design for a lunar mission. We designed a compact custom PCB, shown in Figure 10 to integrate all our chosen components. The components for our robot include a Servocity 60 RPM motor paired with a Pololu breakout board which utilizes a Texas Instruments DRV8874 single brushed DC motor driver. Choosing a lower RPM motor meant we could use less current and increase drive time, which are more critical on the lunar environment than speed. The motor and board are powered by a Tattu 1300 mah 11.1V lithium polymer battery, which should provide the robot with about 1.4 hours of full-throttle run time for each roller. Because a solar panel mount robot like ours will run quite slowly at the lunar south pole, we would expect several days of overall functioning with the current mechatronic system. The motor is controlled via PWM input from an Arduino Nano, which we chose because it provided all the necessary pins for our use-case and has open-source libraries that we used for the radio transmission. For the radios, we chose NRF24L01+ radio modules because of their low weight, power efficiency, long-range adaptor antennas, and integration with Arduino. The PCB also features decoupling capacitors at the input power supply and half-bridge, as well as two diffuse LEDs to provide visual feedback of errors and successful transmissions.

The software emphasizes Object-Oriented Programming (OOP), leveraging shared classes to promote flexible code development with centralized parameters. These parameters, such as node ID and number of children, are the only sections of code modified for each roller. When radio communication begins, an Arduino connected to the base station (the computer performing kinematic calculations) sends movement comman ates with its two child nodes until the entire truss receives the instructions. Checksum errors are embedded within the movement commands to ensure accurate data transmission, and if an error occurs, the child node requests the data to be resent. While a roller is not transmitting data, its DC motor is controlled by a PID controller, adjusting the shape of the truss structure to its desired form.

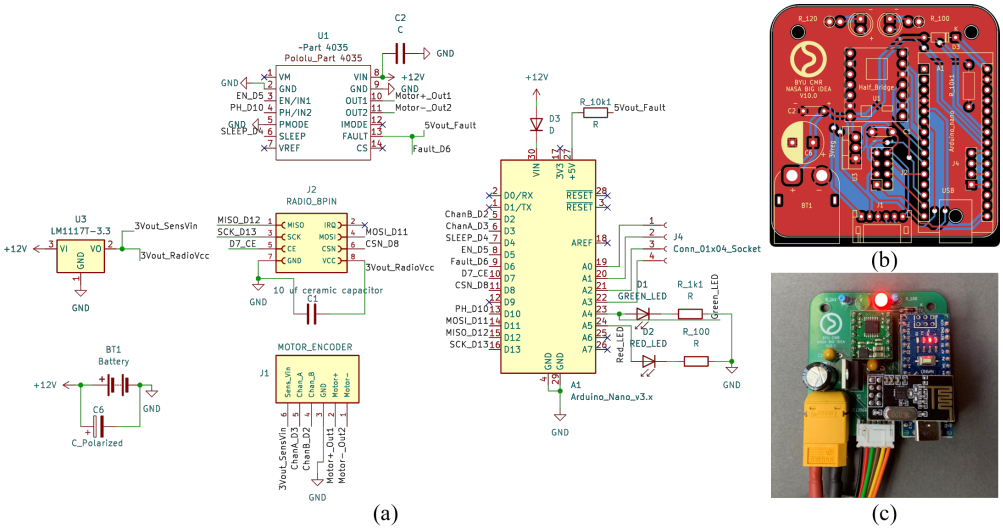

Figure 10: (a) Electrical schematic (b) PCB design. (c) Completed PCB with blue Arduino Nano, green Pololu half-bridge motor driver, and black NRF24L01+ radio transmitter. (motor and battery not shown)

4.5 Kinematics and Dynamics Design

Kinematic Simulation

The original kinematic simulation from the work done in [1] was run using MATLAB. One change that we made to the original simulation was to add additional constraints to the optimizer. These constraints keep the robot from going into a position where the lengths of the edges are too short and avoid singular positions that the robot cannot move out of. We then moved the simulation from MATLAB into Python to better interface with the rest of the control flow. The kinematics were then integrated into the GUI and desired motions are now controlled by a joystick.

Dynamic Modeling

A notable challenge of a soft structure moving significant loads on the Moon is that the motions of the structure tend to be under damped. To address this, we developed a dynamic model which can help us predict and account for the dynamic behavior of the robot. We began by developing the dynamic model for a single node on a single triangle. Each node of the triangle was modeled as a point mass, and each connecting tube was modeled as a linear spring and damper in parallel, as shown in Figure 11.

For our initial simulation, the response of only one node was analyzed. Forces were summed for the top node in the triangle, and equations of motion were developed using a sum of forces approach. We then implemented a 4th-order Runga-Kutta (RK4) integration method in Python, which incrementally updated the position of the node for each time step, and visualized the time-dependent animation using python's MATPLOTLIB library. The inputs to the simulation were gravity and a downward applied force. This method was then adapted to simplify the analysis of more complicated structures.

For each modeled truss, we calculated the rigidity matrix, which details the unit vectors between each pair of nodes, to develop the equations for interactions between the nodes. This allowed for the analysis of multiple nodes, rather than only a single node, and could then be applied to more complicated structures. We developed models for the octahedron, solar array, and crane. These initial models utilized existing kinematic position data only to set the initial position of each node. They assumed that the desired position of each node does not change with time, which was insufficient for analyzing the dynamics of the robot in response to movement commands to the nodes. Thus, our next step in developing these initial models was integrating the kinematic data into the iterative position updates. This was done by utilizing the kinematic, rather than dynamic position data to update the rigidity matrix, resulting in models showing the dynamic response of the truss as follows a predetermined movement path.

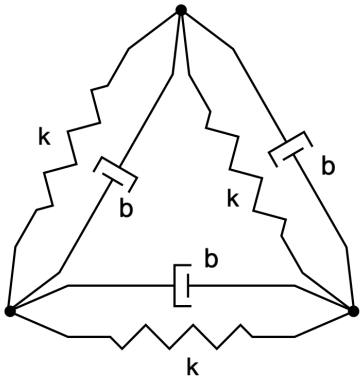

Figure 11: Dynamic model for a single triangle.

5 Conclusion

Permanent human presence on the Moon and beyond requires lightweight and compact infrastructure. Untethered and modular inflatable robots provide an inexpensive, reliable, and versatile way to operate on the Moon. Inflatable truss robots can create solar arrays, unload and transport cargo, and traverse rough terrain. During our burst project, we divided into 4 subsystems - Rollers, Tubes, Joints, and Kinematics and Dynamics - and improved each of them. We constructed a solar array with eight inflated triangles and a mock solar panel and demonstrated its deployment and inflation capability.

6 Verification and Testing

We performed verification to determine if the isoperimetric robot could be adapted to the lunar environment. We tested the deployment and motion of the whole robot together, as well as component testing on each subsystem of the robot. These component tests helped us to refine aspects of the design before the entire robot was complete and verify that each subsystem could integrate successfully together.

6.1 Safety

All tests were performed according to the safety protocols we developed with our University safety officer. This included appropriate use of personal protective equipment, as well as special care ensuring our inflatable systems were operating at safe pressures, and that we followed safety protocols with Lithium Polymer batteries that we used to power the robot. Safety details can be found in our safety plan.

6.2 Full Prototype Testing

We tested the deployment of the robot in two configurations– as a single octahedron, and as a stack of two octahedrons with a solar panel on top. In both cases, the structure was able to deploy with assistance from a human user. When doing our final deployment outdoors, some of the brackets connecting the spherical joints to the rollers yielded mechanically, causing the rollers to bend. The strength of this component can be improved in the future by using stronger brackets.

Roller Testing

One of the key success metrics for our robot's operation on the moon is the amount of run time each roller can go without charging. This metric also relates to the Size, Weight, and Power of our robot, the goal being to minimize size and weight while increasing the power. We selected the half-bridge used to run each motor based on the peak and the average current drawn by each motor. During initial motor and motor-driver pairing tests, we noticed a relationship between the average current draw of each motor and the pressure of the tube. The relationship appears to be linear with a higher current draw corresponding to a higher tube PSI. This is logical because higher PSI exerts a larger force on each roller, causing slight flexing in the rollers and the chassis. This changes the interaction between the Delrin gears, creating more friction and interference. We took some measures to minimize this friction that decreased each motor's average current and lowered the current-pressure relationship's slope. Our robot's mechanical system is well suited to reducing friction, there are no metal interfaces between moving parts. Only metal to Delrin, a rated low-friction material (with a coefficient of friction between 0.1 and 0.3 on steel). Simple measures like adding some lubrication between the gears and between the shafts and the Delrin chassis holes lowered the friction measurably. We also spent a significant amount of time working on optimizing the fit between the components. Minimizing the average current draw is advantageous because it increases the run-time of each roller, improving the efficiency of our design.

Tubes Testing

To ensure that our robot would not have any complications with the tubes, we wanted to evaluate the tubes in their performance under exposure to lunar dust, UV exposure, and how resistant they are to leaks. We also analyzed the complexity of the manufacturing process. We evaluated several candidates and processes, as shown in table 1.

Additional testing was performed on sheets of Neoprene, EPDM, Nitrile, and nylon-reinforced EPDM as we tried to manufacture them into tube form to be utilized for their air-tight properties, but we were unsuccessful in manufacturing these tubes for various reasons. Securing them with multiple adhesives was attempted, as well as melting, heat-sealing, sewing, etc. All of these attempts were unsuccessful at maintaining pressure and shape, so the materials were eliminated from the prospects.

Tube Pressure and Leak Tests Two tubes were pressure tested at various points in the design. The first was an oxford-weave (Denier Nylon) TPU-lined fabric with an LDPE tube. The tube was constructed by heat-sealing the long side of the fabric together, TPU-TPU, to create a long tube, then inserting the liner and heat-sealing the ends. A "+" shaped hole for the valve was cut into the tube on one end and a bulkhead fitting was attached.

Material Name	Sand Blasting	UV Exposure	Manufacturing Process
Polyurethane	=	+	+
200 Denier Nylon	+	+	-
Neoprene	=	=	-
PTFE	=	-	-
Vinyl	=	+	-
Tyvek	-	+	-

Table 1: Summary of the materials evaluated for tubes and the testing procedures. A "+" indicates material performed well,"-" indicates poor performance, and "=" indicates neutral performance.

The tube was pressurized from a compressed air line with inline regulator and pressure gauge. The tube reached a maximum pressure of 17.5 psi before failing due to delamination along the weave of the tube. The tear appeared to start at the hole cut for the bulkhead valve and was 9 inches long. The takeaway from this first test was that the valve in the side was a weak point that limited maximum pressure.

The second static pressure test was conducted on a 2' length of fire hose tubing with FDM 3D printed PLA caps. The fire hose tubing is rated for 150 psi. The tube was placed inside an impact-shielded chamber and connected to a manual bike pump. The air line from the bike pump to the tube was passed through a small diameter hole in the corner of the enclosure.The tube reached a maximum pressure of 50 psi, at which point the test was stopped and the pressure relieved. This test gave us confidence that the tube design with caps and the fire hose tubing would meet the needs for our project.

UV Testing To ensure that the tubing would be able to survive the lunar environment, tests were performed to visually observe degradation from both UV exposure and abrasion resistance/sandblasting (to replicate lunar dust). Materials tested include samples of 200 Denier Nylon, Neoprene, PTFE, Vinyl, and Tyvek.

We performed UV tests in a contained space with samples approximately 10 inches from a UV A/B lamp shining at 365 nm and 240V. The samples were checked every 24 hours for a minimum of 72 hours of exposure and analyzed under a microscope and a visual inspection. Materials such as PTFE that noticeably degraded during this test were eliminated. The TPU coating on the Denier Nylon also degraded slightly, solidifying the firehose tubing as our material choice.

Dust Resistance We evaluated the resistance of the tubing materials to lunar dust by examining how the materials was affected by sandblasting. Sandblasting tests were performed in a metals lab with sandblasting equipment, which was contained in a closed environment and activated by pulling the trigger and pressing a pressure pedal. We held the nozzle approximately 6 inches above the samples and blasted each sample for three minutes using fifteen-second cycles (ten seconds on, five seconds off). We analyzed each sample twice under a microscope, looking at the directly sandblasted region and indirectly affected regions. We eliminated Tyvek immediately after this test since it shredded completely under direct abrasion. The materials shown in Figure 12 are the two recommended for actual use - the 200 Denier Nylon and the single-jacket polyurethane hose.

Thermal Response Testing at Autoliv With collaboration from the Autoliv facility in Ogden, we were able to do some temperature/pressure testing on selected tube materials.

Test 1: Single Triangle In the first tests, we experimented with inflated LDPE inner tubes inside Denier Nylon and Vinyl sleeves in both tube and triangle forms. Temperatures ranged from -40°C to 80°C. These tests were performed by cycling between these temperatures twice each, measuring the data with 6 K-type thermocouples and a pressure transducer. Figure shows13a, and the actual setup is shown in Figure 13. The data from this test is shown in Figure 14.

Unfortunately, the LDPE tubes were not airtight and leaked at the air valves connected to the outside of the tube. We regularly added air to keep the pressure between 1-6 psi, as shown in Figure 14. Thermocouples showed that the internal tube temperatures only varied by 1-3 degrees Celsius from the external

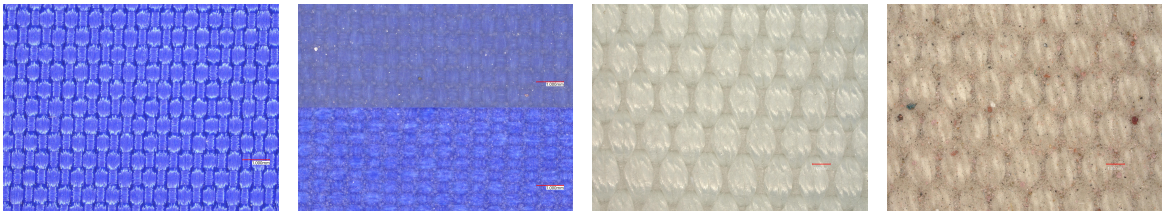

(a) *(b)* *(c)* *(d)*

Figure 12: Comparisons of original samples and the same materials after the sandblasting process. (a) and (b) are the 200 Denier Nylon, and (c) and (d) are the firehose tubing.

-10 pt

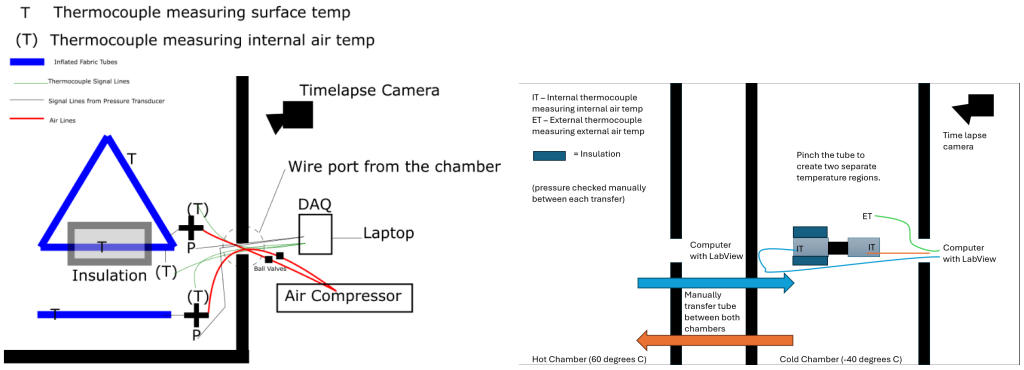

(a) *(b)*

Figure 13: Testing set ups for Autoliv (a) test 1 (b) test 2

temperatures, which matched the chamber temperature. Vinyl and Nylon did not suffer severe degradation from the constant temperature swings. We observed that every cold temperature swing leads to a rapid drop in pressure, even with constant airflow, as shown between 40-50 minutes. Future measures must be taken to pressurize the tube so that cold temperatures do not deflate it, rendering it unusable.

Test 2: Full Octahedron and Instrumented Test Piece The second round of testing at Autoliv experimented on a full octahedron and one small test tube utilizing polyurethane tubing. Each tube was pinched in the middle by a roller module, and the ends were capped with Tough PLA plugs, wrapped with butyl tape for air tightness, and cinched with a circular clamp. We wrapped fiberglass insulation on one side of the test tube to observe two different temperature regions within the same tube. Graphics for the test setup is shown in Figure13b.

We gathered thermal data from this tube on two cold cycles and one hot cycle. On the first cold cycle, the thermocouple measuring the chamber's temperature was stuck in the insulation and had to be adjusted 6 minutes into the test. No significant damage to the fire hose was experienced. Air did leak from the tube at a rate of 0.2-0.5 psi per minute. We suspect this is due to either wear and tear from previous testing or imperfect plug replacement. The polyurethane hose is a far better insulator than the Nylon or Vinyl. At -40 degrees Celsius, it retained a higher internal gas temperature by around 15 degrees Celsius. At 60 degrees Celsius, it retained a lower internal gas temperature by around 10 degrees Celsius. This behavior is advantageous as higher temperatures in cold environments lead to fewer pressure losses. Colder temperatures in hot environments lead to a lower increase in pressure.

We also tested the octahedron for pressure losses. We found that the undamaged triangle member repeatedly returned to the same initial pressure of 5 psi (filled at room temperature) within 3 minutes after removal from a thermal chamber.

While testing the octahedron, we noticed a few points of failure. The format of the parent-child-relay communication to the rollers prevents triangles from being easily detached and replaced. Removing a

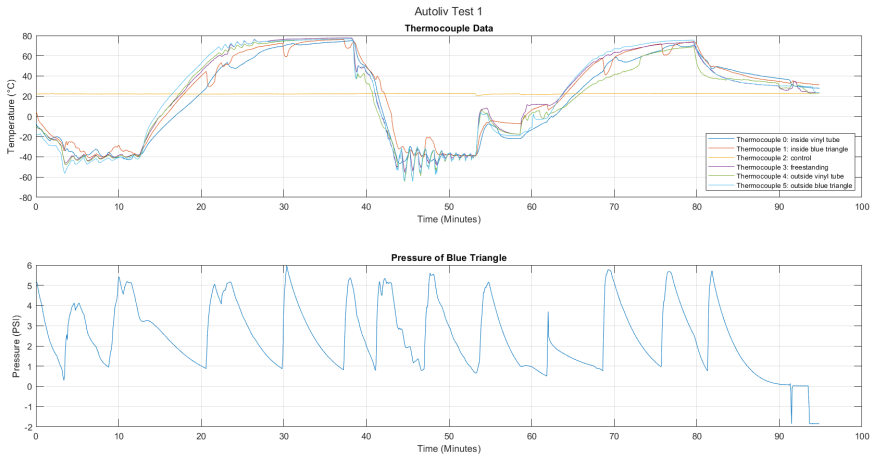

Figure 14: Temperature and Pressure Data of Triangular and Standalone Tube

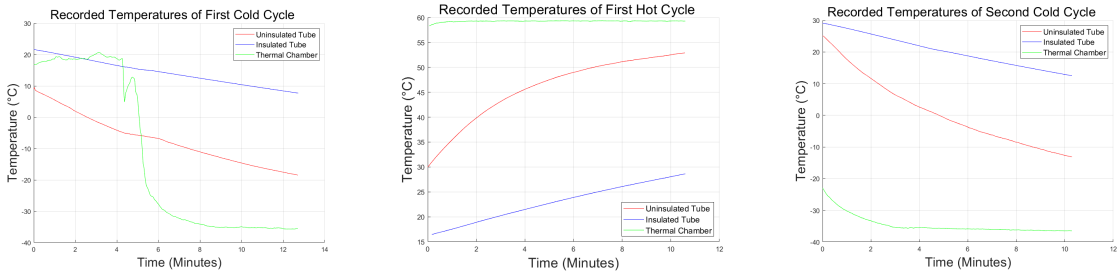

(a) *(b)* *(c)*

Figure 15: Thermocoupler data for (a) 1st cold cycle (Start: 5 psi, End: 0-3 psi) (b) 1st hot cycle (Start: 5.1 psi, End: 3.6 psi) (c) 2nd cold cycle (Start: 15.8 psi, End: 5.9 psi)

single triangle shuts down the communicability and functionality of the whole robot.

Visual inspection revealed severe cracking in two spherical joint spheres due to PLA's temperature limitations. While the cracks did not cause joint failure, we believed their structural integrity was compromised and replaced them after testing completion.

Lastly, we observed two tubes develop leaks during roller operation in the cold chamber. This material weakening occurred due to depressurization and ductile-brittle transitioning at these temperatures. The rollers could not roll properly over the pressure-deflated tube and most likely stretched or tore it attempting to. We suggest pressurizing the tubes to 20 psi (this is a rough guess) in order to have enough pressure in the cold for the rollers to roll along the tube but not enough for it to pop in higher temperatures.

Joint Testing

To validate the functionality of our spherical joint design under loading, we evaluated the joints by measuring their behavior under load and their failure strength. We used a 5 kN Instron tensile tester to assess the strength of a spherical mechanism made of polypropylene and one made of membrane-enhanced PLA. The testing setup is pictured in Figure 17.

In compression, the polypropylene arm deflected until coming into contact with the connector piece (occurred at a compressive load of 46.48 N), which motivated our decision to make the connector piece a sphere so significant compressive deflection would be impossible. In tensile loading, the arm deflected 6.65 cm under a load of 38.47 N. At that point, the panels twisted and one sheared at the hinge. The membrane-enhanced PLA joint failed due to delamination of the membrane under a significantly lower load than the polypropylene joint.

We also connected spherical joints made of PLA to a full-sized octahedron. Rather than shearing at the hinges, as had happened in our tensile and compressive testing, the panels failed due to bending. From

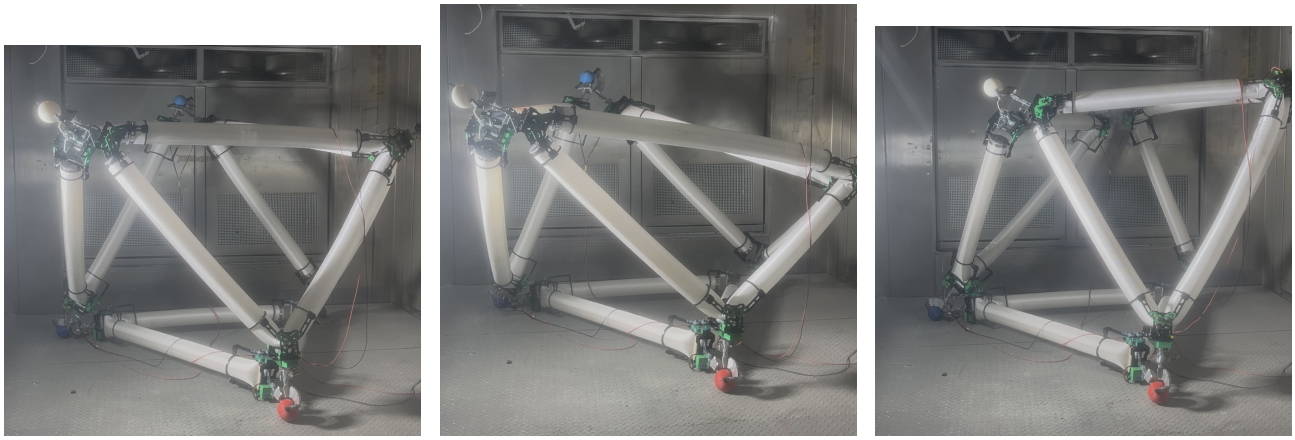

(a) *(b)* *(c)*

Figure 16: Octahedron in Autoliv thermal testing chamber during first cold cycle. The robot is moving under its own power in reponse to radio signals sent from outside the chamber

these tests, we determined that although we achieved the desired range of motion with compliant joints, they would not support the loading required to hold the robot together; we chose to pursue a rigid joint design made of aluminum panels and steel hinge pins.

Mechatronics Testing

To validate our mechatronic system, we developed a test setup to demonstrate the daisy-chaining of movement commands from a root node through a branching tree. This process includes checksum error checking and an auto-acknowledge system to confirm proper reception by each child radio. The latency within this branching structure was about 0.25 seconds of delay per child. When tested with the octahedron structure, the system exhibited quick response times to commands and no data loss during transmission.

We developed a Python-based GUI to allow users to interface and control the robot. The GUI was tested initially with the simulation and then modified to output the kinematic commands to the control node that will relay to each node the desired position along the tube. The GUI has preset configurations for the Octahedron and Solar Array. The user can select the desired node to move and then using a 3-axis joystick move the node to any position in space. During testing we verified and tuned parameters such as input speed, adding direction arrow to know where the desired node is moving, and adjustable output speeds to account for the input to the microcontroller.

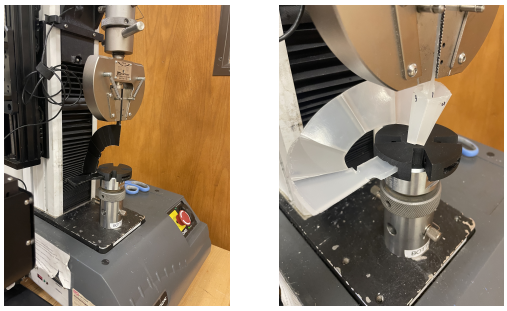

(a) *(b)*

Figure 17: Tensile testing setup. (a) is a membrane-enhanced PLA joint and (b) is a polypropylene joint

Dynamics Testing

To validate the dynamic model we developed, we used three Vive All-in-One VR trackers to collect positional data on the top three spherical joints of an octahedron (see Figure 18). None of the rollers were actuated during the test, which allowed us to collect a basic set of data for how the truss would respond to displacement inputs. The top three spheres were selected for measurement because the bottom of the truss had previously been observed to remain stationary when the top nodes were pushed.

To collect the data, we executed a ViveRos script, implemented in ROS1, that created one node and two topics for each Vive puck. Each node published to 'pose' (position and orientation) and 'twist' (linear and angular velocities) topics. At the start of the test, a ROS bag file was created to record the time-stamped pose and twist data of each ROS message as it was published by each Vive tracker. The duration of the test was approximately 36 seconds with a sampling rate of 1 KHz.

Figure 18: Vive tracker on a spherical joint

The inputs during the test were impulses applied to the top three spherical joints. With the truss in a static state, one of the students would push inward on a spherical joint, forcing it towards the center of the octahedron, then release and allow the truss to reach steady state. We repeated this twice in a rotating pattern on each of the top three nodes. Data was collected continuously for all three nodes during this time.

To begin understanding the results, we re-oriented the base frame for the data to align the z-axis with gravity. This required creating a plane of best fit for the three nodes and using a rotation matrix to rotate all data points into the base reference frame accordingly. This allowed us to view the data in an understandable frame within Cartesian space and is displayed in Figure 19 (a).

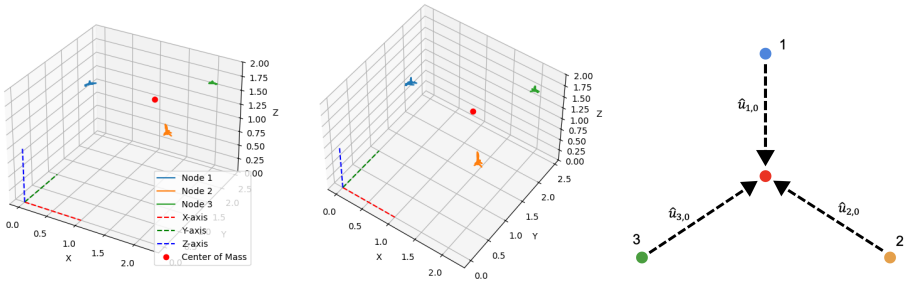

(a) *(b)*

Figure 19: a) Experimental data in 3D Cartesian space for the top three nodes of an octahedron b) node placements and vector directions for initial dynamic analysis

We performed an initial dynamic analysis of the robot by creating unit vectors that extended from the position of each node (1, 2, and 3) to the center of the robot (0), as shown in Figure 19 (b). We used these unit vectors to get the components of the displacement of each node in those directions. This approach was selected as it allowed us to develop an initial, simplified understanding of the coupled response between multiple tubes and joints. One set of results constructed in this fashion is shown in Figure 20 (a).

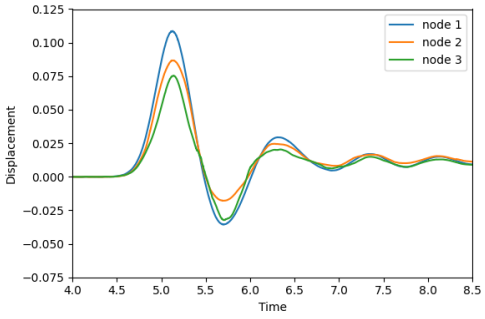

Second Order System Parameters			
Node Projection	ζ	ω_d ($\frac{rad}{s}$)	ω_n ($\frac{rad}{s}$)
$\hat{u}_{1,0}$	0.0673	8.387	8.406
$\hat{u}_{2,0}$	0.0579	8.360	8.374
$\hat{u}_{3,0}$	0.0600	8.433	8.449

(a) *(b)*

Figure 20: a) Representation of unit vector projections of each node along $\hat{u}_{1,0}$ for one disturbance input b) Damping Ratio, Damped Natural Frequency, and Natural Frequency for each node projection

With the data constrained to a single axis, we were able to perform a basic analysis of the frequency response of the system using the log decrement method. The results of these calculations are displayed in Figure 20 (b). From Figure 20 it is clear the robotic truss behaves like an under-damped 2nd order

Figure 21: Rock Canyon elementary visit (left) and on-site event (right)

system, and therefore future work will need to be completed to finish system identification and identify a safe workspace wherein the robot can operate without exciting the natural frequency of the system. It is important to note that while the system parameters are close to the same value in each projection, they do have some variation. This could be attributed to variations in the manufacturing and construction of each roller, joint, and tube, or could be an effect of the octahedron orientation.

6.3 Testing Conclusion

In summation, our research group completed verification testing on both subsystems of the robot and the combined system. We determined that the combined robot behaved like a second-order system when driven with an impulse. We tested the final spherical joints in various stress orientations by moving the robot and while assembling the robot. We tested a single octahedron of the robot in a temperature chamber at Autoliv and examined the effect of temperature swings on all components of the robot. Finally, we assembled the robot with a mock solar panel on top, in the configuration outlined in our project proposal. Although each one of these tests demonstrated vulnerabilities in our final prototype, we are satisfied with our progress toward creating a more lunar-ready robot. Each subsystem has undergone significant improvement from where it began, and though we didn't have the time to finish all the testing we outlined in our original proposal, we are satisfied with our current results. Recommendations for continued testing can be found in Path to Flight.

6.4 Outreach

We participated in two outreach events with elementary school-age students during this project. This was part of our proposal to ensure that our project contributed to diversity, equity, inclusion, and STEM. The first took place at Rock Canyon Elementary School in Provo, UT, during September. For the event, five students traveled to the school with a collection of assembled components from the robot. The goal of the event was to help the participating elementary students gain a better understanding of the engineering design process and how it was applied to this project.

A total of approximately 50 2nd grade students participated, split between two classes that each lasted for 30-40 minutes. During that time, our presenters discussed how engineers creatively solve problems based on the constraints they're given, with illustrations from the tubes, rollers, and spherical joints from this project. As part of the presentation, each student was able to help pump up one of the truss's tubes to illustrate the advantages of a deployed inflatable structure (See Figure 21). At the end of the sessions, each elementary student received 3D printed components that could be assembled into a mini version of the full-size robot they had just learned about. We received feedback after the event that the students had thoroughly enjoyed the opportunity to interact with our volunteers.

The second outreach event also happened in September, when one of the CMR graduate students brought in a group of elementary-age girls from their neighborhood to learn about opportunities for women in STEM (See Figure 21). Fortunately, because the visit happened on-campus and the students could visit our lab, this event was much more interactive. The girls were able to ask more questions, both about engineering and about the project, and had the benefit of seeing the assembled system. We also gave each girl the opportunity to assemble a mini octahedron as we had at Rock Canyon, with similar enjoyment and excitement.

7 Path to Flight

7.1 Rollers

For the roller design to be fully prepared for use in a lunar environment, the Delrin chassis will need to be replaced with a space-grade material, such as an aluminum alloy. Changing the chassis material would necessitate two key design changes to the roller; introducing the need for bearings or bushings in the shaft connections, and eliminating the need for three separate chassis pieces. We chose to make the chassis out of Delirn because it is a self-lubricating material and is easy to laser cut and post-process. We found that Delrin would not be able to withstand the fluctuations in temperature the robot would experience in space flight and on the moon.

The addition of an extra component for the rotating interface between the shafts and the chassis also brings with it increased failure points. Bearings and bushings would need to be sealed against the abrasive substrate to increase their lifespan, otherwise the increased wear could lead the shafts to lock up and become unusable. Even if operation could continue with the magnified resistance, the system's overall efficiency would drop as a result.

Fortunately, in switching to a metal chassis, the fact that such materials can be manufactured in rectangular pipes can be taken advantage of to improve the precision of the roller dimensions. This can be done by starting with a rectangular pipe of proper base dimensions, then using a CNC machine to create the entire chassis from one piece. This will ensure that holes for the shafts are properly aligned and also reduce the overall part count because there will no longer be a need for connecting screws between the chassis pieces.

7.2 Tubes

Future testing recommendations for the tubes include electrostatic testing, refining the plug design, switching tubing, and load analysis and testing.

Further recommended research includes determining the electrostatic properties of the tubing materials, as the lunar regolith is electrically charged. With help from Dr. David Allred and Josh Vawdrey at the BYU Physics Department, we were trained to use and adapt a contamination chamber to expose the tubes to charged dust as a simulated environment. The chamber is set to 70 mTorr of pressure, and the dust is electrically charged to imitate the triboelectric charge experienced by lunar dust. By rolling the tube along the dust, we could test solutions to repelling charged dust along the tube.

The current plugs are made from SLA resin and printed on a Formlabs 3D printer. SLA resin has poor performance characteristics at low and high temperatures and low UV resistance. The final plug material could be selected from aluminum or acetal, which have much better UV and temperature resistance and less porosity. Both are available in 4" bar stock, allowing for machining via 4-axis CNC.

The current polyurethane tubing from Schraiberpump failed under cold operating conditions. We propose switching to a single-jacket polyurethane hose with an inner EPDM coating. EPDM responds better in extreme temperatures and would provide an additional layer of protection against puncture or tear.

Our proposed use cases for the robot involve having the ability to carry or move weight. To ensure the robot is capable of its intended uses, we want to test its ability to carry and manage different loads through load testing. The only load testing completed was with a mock solar array; further testing is highly recommended.

The primary goal would be testing the robot's ability to support and stabilize various weights placed on top of the solar panel in the solar array. This information will show how much weight the robot can adequately function with and confirm our models. We specifically want to identify any instances of buckling, shifting, or strain on joints or nodes so we can make any necessary adjustments, such as making the walls of the tubes thicker, increasing pressure, or strengthening the design of our joints or nodes. We hope to explore different sizes and weights of solar panels we can use and learn more about their weight-bearing abilities. This testing will also allow us to make any design adjustments necessary to ensure the robot is strong enough to reliably carry solar panels or other weights that we envision it will be able to do.

7.3 Joints

The spherical joints on the demonstrator robot use a series of pin joints to create the "arms". However, these pin joints are susceptible to damage and losing range of motion from lunar dust. To mitigate the effects of

the dust, we are planning to design a sleeve to fit over each hinge, which would be made from the same material as the tubes (i.e. capable of repelling dust). Such a sleeve would impede dust from "freezing" the joints and increase the joint durability.

As mentioned in the section on joint design, we have future work planned to develop a fully compliant spherical joint. We will continue to develop better membrane hinges, improving on the work we have done. Membrane hinges often suffer from parasitic motion, but this can be mitigated by rigid geometries that restrict undesirable motion. An alternative compliant design involves Compliant Rolling Contact Elements (CORE) [8] as hinges connecting truncated cones to create a spherical arm. Tensioned steel bands will be used as the connective bands in the CORE joints. These remove the need for lubricating hinges and reduce backlash and parasitic motion. While compliant mechanisms themselves may be less susceptible to damage from lunar dust, all of these designs may also incorporate a sleeve for additional protection.

The material used for the central, spherical joint connection is currently 3D-printed PLA carbon fiber, which is not space-grade. We plan to pivot to a hollow steel sphere.

7.4 Mechatronics

A major concern for electronics on the lunar surface is the effect of ionizing radiation. All electronics are susceptible to impact from high-energy particles that cause Single Event Effects, which can flip bits, affecting computing system calculations. To ensure that ionizing radiation does not change these calculations, most spacecraft employ multiple identical systems that compare calculations and use a "majority voting" system to determine the correct calculations. This is an option for our system as well, as additional microcontrollers can be included on the PCB for minimal added cost, weight, and volume.

Another concern for the electronics is the recommended operational temperature range of standard Arduino microcontrollers: -25°C to 70°C. This range resides close to the thermal range expected in the lunar environment but would still place the circuitry of the system at risk of permanent damage. As such, we recommend some form of electronic thermal shielding. Because the dominant heat transfer mechanism on the moon is radiation, the ideal shielding would be one that both absorbs and emits very little thermal radiation such as aluminum. This would reduce the rate of heat transfer to/from the electronics at both temperature extremes, reducing the maximum temperatures experienced during a lunar cycle.

The current Lithium Polymer (LiPo) batteries have a large number of risks associated with them, the least of which is a reduced lifecycle when not handled properly. The current PCB does not implement a cell-balance discharge system, ensuring each cell discharges at the same rate as its neighbors, nor do the electronics monitor the battery voltage to protect against over-discharging. Both concepts would be strongly recommended to improve the lifespan of the current and future batteries.

An alternate battery chemistry such as Lithium Ion would improve the lifespan and capacity of the batteries, but at the expense of the consequences of a battery failure such as a thermal runaway event. Lithium Iron-Phosphate (LiFeP04) batteries are much safer in that regard, with comparable lifecycles, but come at the cost of lower energy density.

7.5 Dynamics

The existing dynamic model can be adjusted to simulate moon gravity instead of earth gravity. However, there are additional revisions that could help track the physical behavior of the system more closely.

An alternate dynamic model could implement torsion springs and dampers at each node, as opposed to the current axial approach. This could greatly improve the performance of the model, as the physical system has consistently demonstrated the greatest compliance at the node connections.

A more complex alternative model could be developed in a physics-based robotic simulation software, such as MuJoCo. This would enable improved ground contact simulation for both earth and moon gravity and would also present an interesting foray into soft robot simulation within a traditionally rigid-body simulation tool.

Additional data will be needed to identify the physical parameters of the system, regardless of the model used in simulation. However, once the physical parameters are known and the simulated system consistently behaves similarly to the physical one, there is the possibility of developing input shaping for commands to the robot based on the expected frequency response of different commands. This could be further enhanced by placing inertial measurement units (IMUs) on each joint and/or roller of the robot, allowing for a closed-loop controller to be developed that actively cancels vibrations induced during movement.

8 Project Management

8.1 Team Leadership and Management Approach

This burst project has been entirely student-led and developed. Because our robot could easily be broken into 4 different sub-systems, we structured sub-teams around those systems and our leadership and management approach around those sub-teams. Each sub-team consisted of one or two graduate students and up to ten undergraduate students. One of the graduate students was chosen as the leader of each sub-team and would organize weekly or bi-weekly team meetings to discuss progress and next steps. Accountability for deadlines and assignments was handled by the sub-team leaders, who often used physical calendars as well as digital reminders to help their teammates. For communication, team members used a variety of options including text message, Microsoft Teams, and Outlook emails.

All sub-team leaders also met weekly with each other, the faculty advisor, and an overall project coordinator to discuss the overall state of the project, coordinate work on deliverables, and make high-level design decisions. All major decisions were made by appointing someone on the specific sub-team to research the topic, and then they would report back with their findings to their sub-team and thus with all the team leads. The sub-team would brainstorm potential solutions together and test/prototype different approaches, eliminating potential decisions through experimentation, reasoning, or inability to purchase or afford a solution.

This process of design space expansion and contraction was repeated many times on each sub-team, along with advice and insight from the other sub-teams as the opportunity arose. Purchasing decisions were made only after consulting with the sub-team during sub-team meetings, or in emergencies approved by one or more of the sub-team leaders over Teams message. Every purchase request was also reviewed by the faculty advisor before being approved.

8.2 Project Schedule, detailed timeline

See Figure 22.

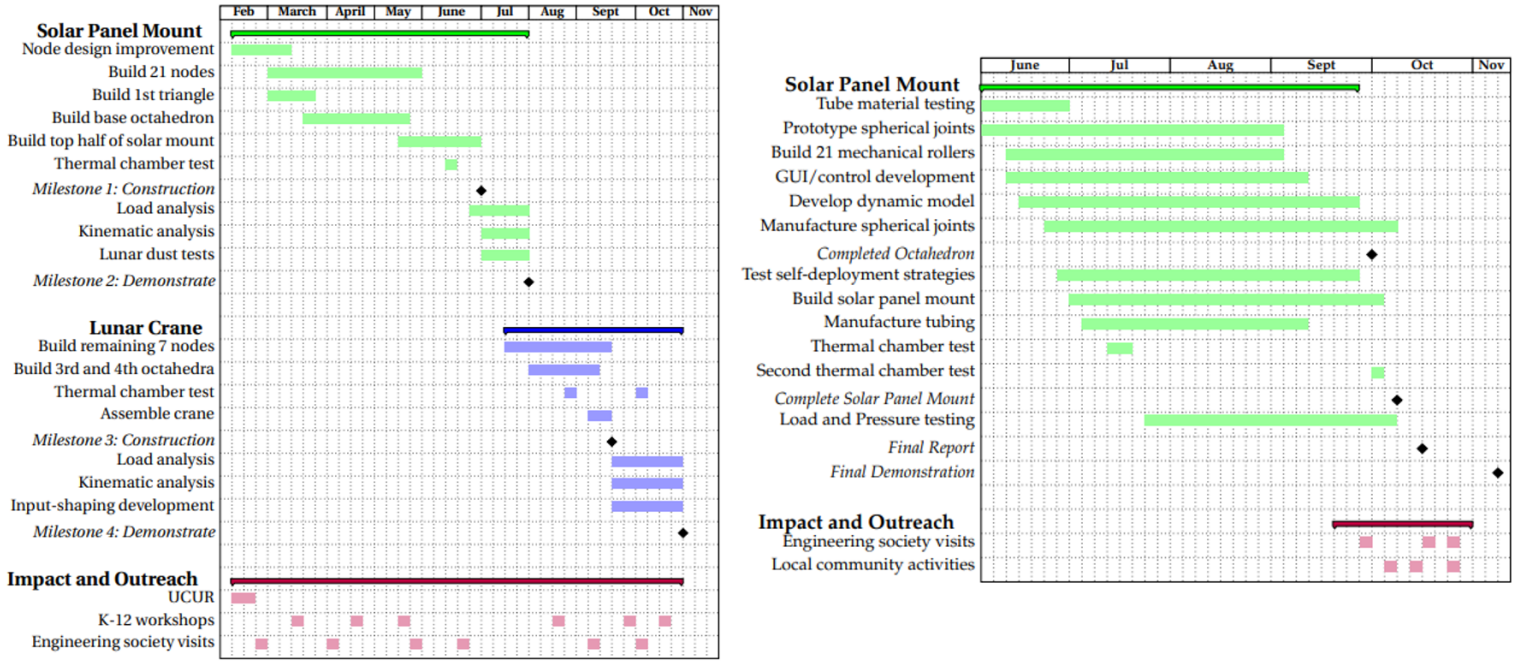

Figure 22: Comparison between original proposed timeline (left) and actual timeline (right)

8.3 Budget

Our budget expenditures are shown in Figure 23.

Category	Initial Budget	Spending as of Oct. 1	Expected
Student Salaries and Benefits	$107,190.00	$72,696.54	$30,000.00
Autoliv Testing	$7,200.00	$4,950.00	$0.00
Materials	$21,360.00	$26,759.82	$2,000.00
Travel	$12,090.00	$3,000.00	$5,000.00
LSIC Registration			$800.00
Total Budget	$147,840.00	$107,406.36	$37,800.00
		Expected Total:	$145,206.36

Figure 23: Budget expenditures over the course of the project

Our strategy for making decisions about purchases was dividing our supply team based on subteams. We started with each team subteam having a budget, and then moved funds between teams as overall demands changed.

Two challenges we faced were in managing team size and dealing with procurement delays. We started with a small team and grew to a large size, meaning that we initially were spending money below our budgeted amounts. Towards the end of the project, we had to spend more money to procure parts with shorter lead times in order to continue development. We did not receive any funding in addition to the BIG Idea award.

References

[1] N. S. Usevitch, Z. M. Hammond, M. Schwager, A. M. Okamura, E. W. Hawkes, and S. Follmer, "An untethered isoperimetric soft robot," *Science Robotics*, vol. 5, no. 40, p. eaaz0492, 2020.

[2] M. Wehner, M. T. Tolley, Y. Mengüç, Y.-L. Park, A. Mozeika, Y. Ding, C. Onal, R. F. Shepherd, G. M. Whitesides, and R. J. Wood, "Pneumatic energy sources for autonomous and wearable soft robotics," *Soft robotics*, vol. 1, no. 4, pp. 263–274, 2014.

[3] J. D. Madden, "Mobile robots: motor challenges and materials solutions," *science*, vol. 318, no. 5853, pp. 1094–1097, 2007.

[4] M. LLC. (2024) Material properties chart. [Online]. Available: https://www.martins-rubber.co.uk/technical-references/material-properties

[5] R. Kovacs, A. Ion, P. Lopes, T. Oesterreich, J. Filter, P. Otto, T. Arndt, N. Ring, M. Witte, A. Synytsia *et al.*, "Trussformer: 3d printing large kinetic structures," in *Proceedings of the 31st Annual ACM Symposium on User Interface Software and Technology*, 2018, pp. 113–125.

[6] A. Spinos, D. Carroll, T. Kientz, and M. Yim, "Topological Reconfiguration Planning for a Variable Topology Truss," *Journal of Mechanisms and Robotics*, vol. 13, no. 4, p. 040902, 04 2021. [Online]. Available: https://doi.org/10.1115/1.4050530

[7] ——, "Variable topology truss: Design and analysis," in *2017 IEEE/RSJ International Conference on Intelligent Robots and Systems (IROS)*, 2017, pp. 2717–2722.

[8] P. A. Halverson, L. L. Howell, and S. P. Magleby, "Tension-based multi-stable compliant rolling-contact elements," *Mechanism and Machine Theory*, vol. 45, no. 2, pp. 147–156, 2010. [Online]. Available: https://www.sciencedirect.com/science/article/pii/S0094114X08002383